Pergamon

Int. J. Heat Mass Transfer. Vol. 37, No. 15, pp. 2245–2259, 1994

0017–9310/94 $7.00 + 0.00

0017–9310(94)E0038–V

A study of bubble ebullition in forced-convective subcooled nucleate boiling at low pressure

E. L. BIBEAU and M. SALCUDEAN†

Department of Mechanical Engineering, The University of British Columbia, Vancouver, B.C., Canada V6T 1Z4

(*Received* 23 *April* 1993 *and in final form* 24 *January* 1994)

Abstract—An investigation of forced-convective subcooled nucleate boiling was carried out using high speed photography. Experiments were performed using a vertical circular annulus at atmospheric pressure, for mean flow velocities of 0.08–1.2 m s^{-1} and subcoolings of 10–60°C. The filmed conditions are defined relative to the onset of nucleate boiling and the onset of significant void. The following observations were made: (i) bubbles do not grow and collapse on the heated wall, but eject into the flow for subcoolings below 60°C; (ii) after the onset of nucleate boiling, bubbles slide away from the nucleation site and later eject into the flow; (iii) bubbles condense while sliding on the wall; and (iv) bubbles generated near the onset of nucleate boiling conditions slide for a distance of up to 50 mm, while for other conditions the total axial distance traversed by the bubbles is less than 2 mm on average. The maximum bubble diameter and condensation time are shown to be influenced by the location relative to the onset of significant void.

1. INTRODUCTION

AN IMPROVED understanding of the bubble ebullition cycle in forced-convective subcooled nucleate boiling conditions is important for modeling void growth and heat transfer. Many models of void growth are based on bubble behavior [1, 2]. Heat transfer mechanisms can be better understood through studying the bubble ebullition cycle. For instance, it may be possible to determine whether the heat transfer is governed by the increase in the micro-layer evaporation under the bubble due to the sliding of the bubble, as suggested by Tsung-Chang and Bankoff [3], or by the stirring at the wall, caused by the replacement of liquid behind the detaching bubble, as suggested by Rohsenow and Clark [4].

Many experimental studies have investigated the bubble ebullition in forced-convective subcooled nucleate boiling at near atmospheric pressure. Gunther [5] performed a photographic study of surface boiling for T_{sub} = 15–65°C, U = 1.5–12.2 m s^{-1} and P = 1–11 bar. The test section was a rectangular channel (4.8 × 12.8 × 152 mm), divided in mid-plane by an electrically heated metal strip (0.1 mm thick and 3.1 mm wide). Gunther reported that, at high subcooling (T_{sub} > 38°C), bubbles were hemispherical, grew and collapsed while sliding along the heater, and did not detach from the surface. The bubble sliding velocity was approximately 80% of the mean flow velocity. Rohsenow and Clark [4] analysed high-speed motion pictures of McAdams *et al.* [6] for a heated annulus for U = 1.3 m s^{-1}, P = 2 bar, and T_{sub} = 10–66°C, and found that bubbles were ejected into the fluid core where they condensed rapidly. The motion of bubbles moving into the liquid core caused violent agitation of the liquid near the surface and enhanced the heat transfer rate. Bubble traces and bubble photographs have been reported by Stralen [7] for flow velocities between 3 and 6 m s^{-1} and subcoolings of 5–35°C at atmospheric pressure. Traces show that the bubbles are elongated when ejected into the flow. Photographs show that bubbles slide along the wall prior to ejection, and small, residual bubbles are present in the flow. Akiyama and Tachibana [8] studied bubble growth and collapse using an annulus for U = 0.1–5.0 m s^{-1}, P = 1 bar, and T_{sub} = 20–80°C. In their study, bubbles, either near-spherical or slightly flat in shape, slide on the wall, subsequently detach into the liquid core, and then condense. Before detaching, the bubbles start to condense on the wall while sliding. The photographs shown in their investigation are too small to allow the reader to draw definite conclusions on bubble shape and displacement. Del Valle and Kenning [9] investigated subcooled nucleate boiling on a stainless steel plate for U = 1.7 m s^{-1}, P = 1 bar and T_{sub} = 84°C. Bubble life times were less than 0.6 ms. They observed that the majority of the bubbles grow and collapse at their own nucleation sites, and only a few bubbles slid along the wall. At elevated pressures, photographic studies by Dix [10] (P = 3.1–8.4 bar) and Unal [11] (P = 1–16 bar) showed that bubbles do not adhere to the wall. They are located in the liquid core [11], and travel in a narrow bubble layer close to the wall [10].

† Author to whom correspondence should be addressed.

NOMENCLATURE

D_n	bubble diameter normal to the wall [m]	T_{onb}	temperature at the onset of nucleate boiling [°C]
D_p	bubble diameter parallel to the wall [m]	T_{sub}	subcooling [°C]
L_n	normal displacement [m]	t	time [s]
L_n^*	L_n minus L_n at ejection [m]	t_b	bubble lifetime [s]
L_p	parallel displacement [m]	t_g	time for bubble growth period [s]
L_{Ptotal}	parallel displacement from inception to collapse [m]	t_c	bubble condensation time [s]
l_{Pej}	parallel displacement from ejection to collapse [m]	t_n	time for bubble necking period [s]
$\dot{m}$	mass flow rate [kg s^{-1}]	t_p	bubble period [s]
P	pressure [kPa]	U	mean flow velocity [m s^{-1}]
R_b	bubble volume equivalent radius [m]	u_b	bubble sliding velocity [m s^{-1}]
R_{max}	maximum bubble volume equivalent radius [m]	u_{ej}	bubble ejection velocity [m s^{-1}]
S	velocity slip ratio [u_b/U]	V_b	bubble volume [m^3].
T_{fdb}	temperature at fully-developed boiling [°C]	Greek symbols	
T_{in}	inlet temperature [°C]	ϕ	heat flux [W m^{-2}]
		θ_a	advancing contact angle [°]
		θ_r	receding contact angle [°].

High speed photographic studies report different bubble behaviors, depending on the subcooling and velocity, and there appear to be some contradictions under similar conditions. In general, bubbles collapse on the wall at high subcooling, while, at low subcooling, bubbles are ejected into the fluid core and condense. Gunther's results, which apply only to high subcooling (above 38°C), are sometimes used to describe the behavior of bubbles throughout most of the subcooled boiling region, as in Cole [12], who wrote, "In subcooled boiling, the bubbles generally do not depart from the heated surface but instead grow and collapse on the surface".

The onset of significant void, OSV, is an important parameter in void growth studies as it marks the location where a small change in power causes a substantial increase in the void fraction value, as shown in Fig. 1. The highly subcooled region occurs between the onset of nucleate boiling, ONB, and the onset of significant void, OSV (Fig. 1). Most void growth models assume that, in the highly subcooled region, bubbles grow and collapse on the wall, either without sliding [13] or with sliding [14]. This contradicts photographic studies at elevated pressure [10, 11], which report bubbles migrating towards the liquid core in this region. The photographic studies reported in the literature do not describe the bubble behavior in relation to the OSV.

The objective of this work is to perform a photographic study of subcooled boiling at low pressure and low flow rate, in order to provide a more quantitative description of the bubble growth and collapse, and to examine how the bubble detaches from the wall.

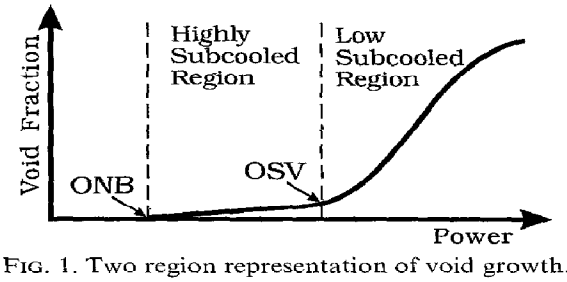

FIG. 1. Two region representation of void growth.

2. EXPERIMENTAL APPARATUS

The high speed photographic study of forced-convective subcooled boiling at atmospheric pressure was obtained using an experimental two-phase loop, shown in Fig. 2. A forced convective flow is generated past an internally-heated annular test section by a

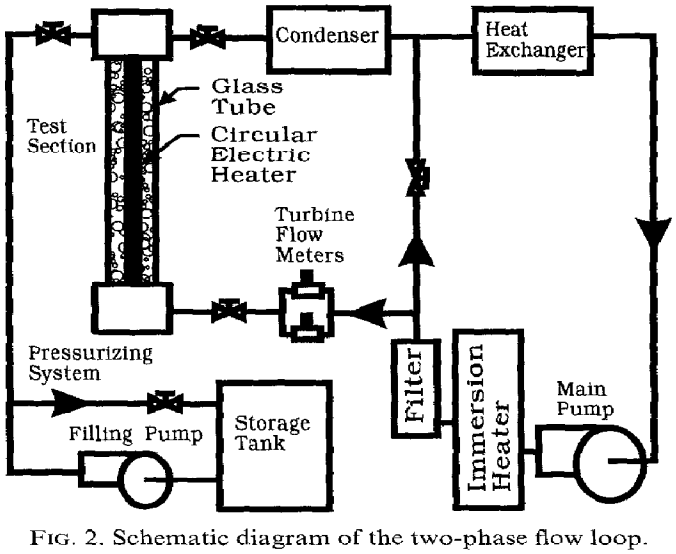

FIG. 2. Schematic diagram of the two-phase flow loop.

closed-loop system, consisting of the following components: main pump, immersion heater, filter, turbine flow metering system, flow control valve, heated test section, vertical cross-flow condenser, and heat exchanger. The water in the loop is preheated to 100°C to de-gas the water, while trapped air is periodically removed from the condenser or the immersion heater.

The vertical test section consists of a circular heater electrically heated by a 64 kW a.c. low voltage power supply, and an outer Pyrex glass tube. The circular heater, 480 mm long and 2.1 mm thick, was fabricated from a 304 stainless steel 12.7 mm dia. tube, silver-welded at both ends to thick wall copper tubes. The diameter and length of the heater is identical to an actual fuel element used in the SLOWPOKE reactor, while the 22 mm glass tube I.D. was chosen to provide an equivalent hydraulic diameter simulating the flow past a single fuel element.

The volumetric flow rate was measured with two turbine flow meters, the current and the voltage drop across the heater were measured for heat flux calculations, and the inlet temperature was measured with K-type ungrounded thermocouples. The instrumentation was interfaced with a 486 IBM compatible computer.

High speed photography was performed using a Hycam (Model #K2054E) at film speeds between 5000 and 6000 frames s^{-1}. Figures 3 and 4 show the experimental and film digitizing setups, respectively. An 8 mm long section of the annular flow passage from the heated wall to the glass tube was filmed on each frame at an axial location of 440 mm along the heated element (Fig. 3). A 1.0 magnification of the image was achieved by using a 35 mm telephoto lens (focal length 80 mm at f/2.8) with a 40 mm extension tube. The depth of field is approximately 4 mm. The film was eventually converted into a video signal using a solid state CCD camera system (Tamron/FotovixII) which enlarges the image up to 36×. Each image was digitized using a 640×480 frame grabber (PcVisionplus-640-3-60).

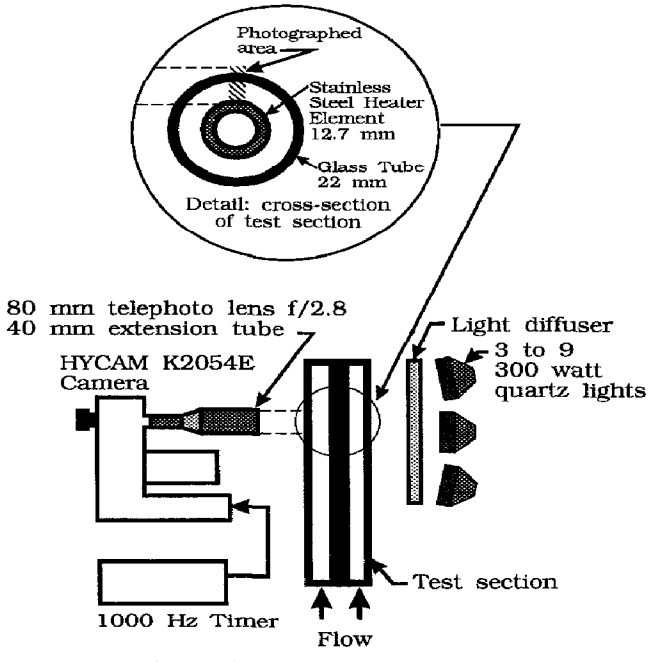

FIG. 3. High speed photography experimental setup.

Encoded on the high speed film is a constant frequency time mark of 1000 Hz. Two perpendicular lines etched on one of the mirrors in the Hycam were photographed on each frame. These lines provided an accurate reference frame. In addition, a precision ruler located beside the glass tube was photographed to determine the scaling of the image.

An interactive computer program developed by Farajisarir [15] was used to analyse the 20–40 digital bubble images in each bubble ebullition cycle. All the bubbles digitized within an ebullition cycle grew and collapsed within the photographed 8 mm length of the heater. Inputs to the program were provided by "clicking" with a computer mouse at the appropriate location on the computer screen. These inputs include: the location of the nucleation site; the location of two points 6 mm apart along the precision ruler; the location of the fixed reference frame for each digitized bubble image; and the location of the time marks. In addition, the outline of each bubble was traced with the computer mouse. The area, the center of mass, and the principal axes of inertia were then computed from the bubble outline.

The program then calculated the following parameters, shown in Fig. 5: the diameter of the bubble along the principal axis of inertia, parallel to the wall, D_p, and normal to the wall, D_n; the bubble advancing angle, θ_o, and receding angle, θ_r; the parallel displacement of the center of the bubble with respect to the nucleation site, L_p; the normal displacement of the center of the bubble with respect to the wall, L_n; the elapsed time, t; the bubble volume, V_b; and, finally, the bubble volume equivalent radius, R_b.

The bubble volume was obtained by averaging two volumes, calculated as follows: the two areas located on each side of the minimum axis of inertia are revolved separately about the axis, thus creating two bodies of revolution. Their volumes are then averaged to obtain V_b. The volume equivalent radius is by definition:

$$R_b = \left(\frac{3V_b}{4\pi}\right)^{1/3}. \quad (1)$$

The reference mark on each photographic frame is used to measure accurately the displacement of the center of mass of the bubble with respect to the nucleation site and the heated wall.

A detailed description of the photographic study can be found in ref. [15].

Measurement errors, listed in Table 1, were obtained from specifications provided by the manufacturer or estimated from experiments. The accuracy of the measured bubble parameters (Fig. 5) was limited by the pixel size of the digitized image, as dis-

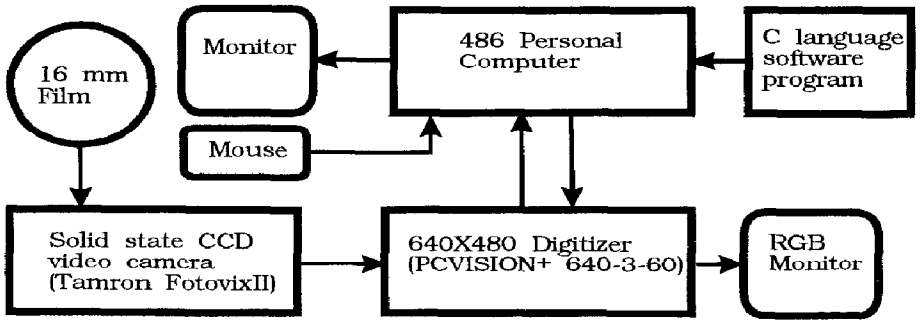

FIG. 4. High speed photography film analysis setup.

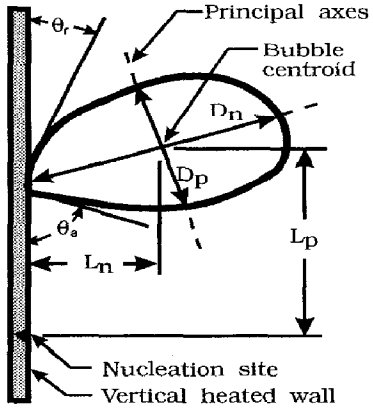

FIG. 5. Bubble parameters measured from the digitized image.

Table 1. Estimated error for experimental parameters

Parameter	Error (±)
Inlet pressure, P	140 Pa
Inlet temperature, T_{in}	1.0°C
Flow rate, $\dot{m}$	0.3%
Heat flux, ϕ	1.8%
Parallel diameter, D_p	0.1 mm
Normal diameter, D_n	0.1 mm
Parallel displacement, L_p	0.1 mm
Normal displacement, L_n	0.1 mm
Time, t	0.02 ms
Bubble radius, R_b	1.6%
Bubble volume, V_b	5.0%
Contact angles, θ_a and θ_r	10°%

cussed in ref. [15]. Although the bubble image is magnified 36× on the computer screen, contact angles were hard to determine accurately due to the reflection of the bubble base on the stainless steel heater.

The input parameters for the high speed photographic study were heat flux, subcooling, and flow rate, as shown in Table 2. Figure 6a–e shows the conditions for each film for subcoolings of 10, 20, 30, 40, and 60°C. Each condition is given a reference number (e.g. D23). Figure 6a–e also shows the relative location of each condition filmed with respect to the onset of nucleate boiling (ONB), and the onset of significant void (OSV), both of which were calculated using correlations previously developed by Bibeau *et al.* [16]. Films were obtained for conditions within the highly subcooled region, near OSV, and after OSV. Conditions which require the inlet temperature to be less than 15°C are indicated in the figures, since this value corresponds approximately to the minimum water temperature attainable in the experimental loop used. Fewer conditions are available for filming for values of high subcooling and low flow rate. Films obtained at a subcooling of 60°C were intended to determine whether or not bubbles condense at high subcooling while still attached to the wall, as described by Gunther [5].

Table 2. Input parameters for high speed photographic study

Input parameter	Range
T_{sub} (°C)	10, 20, 30, 40, 60
$\dot{m}$ (kg s^{-1})	0.02, 0.10, 0.20
ϕ (MW m^{-2})	0.1–1.2
P (bar)	1.05

All photographic films were obtained with the same stainless steel heater element and at the same camera location. From two to eight different nucleation sites were identifiable for each film, depending on the heat flux. Only bubbles produced at the same active nucleation site were digitized (by Farajisarir [15]), and 5–10 bubbles were digitized from each film. Choosing the same nucleation site eliminates variations in bubble size due to different cavity sizes. For the film speed used in this investigation, the bubble life cycle—from nucleation to bubble collapse—was captured on 20–40 frames, and for a subcooling of 60°C and pressures of 2 and 3 bar, the bubble life cycle was captured on 4–10 frames.

Additional information on the experimental apparatus and the high speed photographic study can be found in Farajisarir [15] and Bibeau [17].

3. RESULTS AND DISCUSSION

Figure 7 shows the digitized bubble radii as a function of time taken from the same film and the same nucleation site for condition reference DO6. The figure shows that the growth rate is the same for all bubbles, although the maximum radius and bubble lifetime varies from bubble to bubble. A 'typical bubble' is selected from each film which has the bubble lifetime closest to the computed average lifetime of all the digitized bubbles.

Some nucleation sites become temporarily inactive

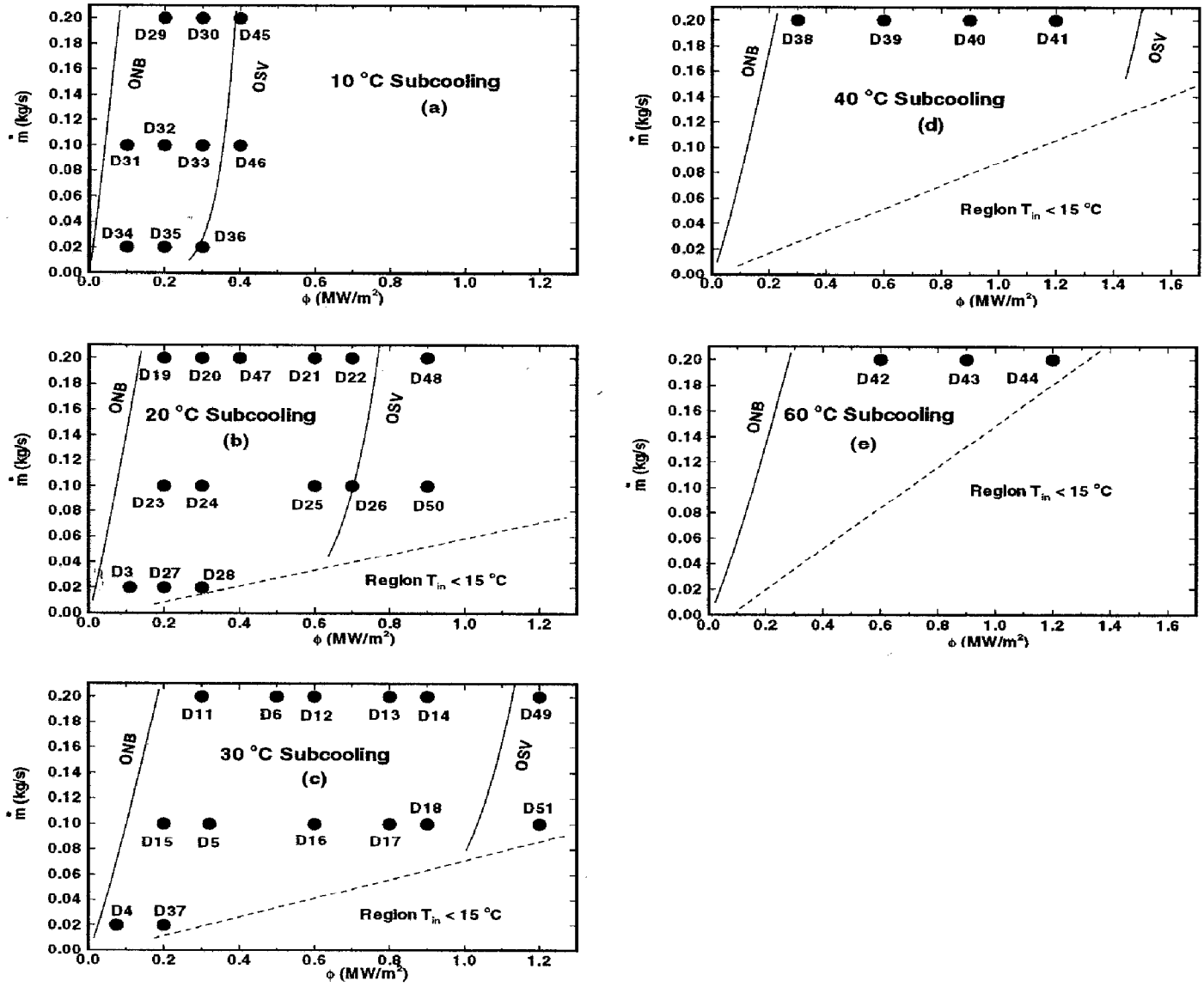

FIG. 6. High speed photography filmed conditions with reference numbers for subcoolings of: (a) 10; (b) 20; (c) 30; (d) 40; and (e) 60°C, and flow rates of 0.02, 0.10 and 0.20 kg s^{-1}. The onset of nucleate boiling, ONB, and the onset of significant void, OSV, are also shown.

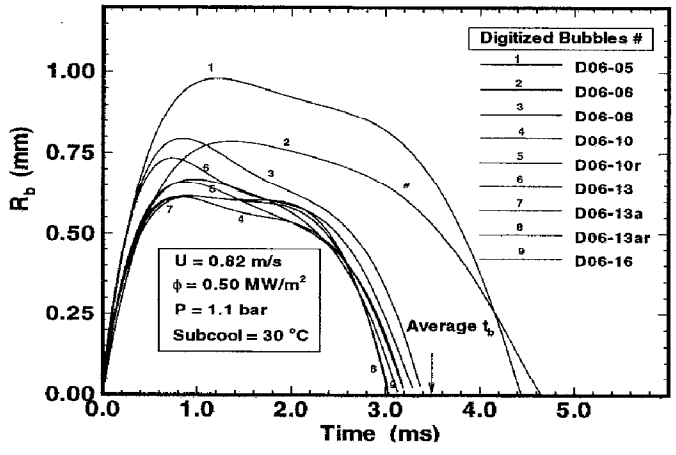

FIG. 7. Different digitized bubble radii for reference condition D06.

over a range of heat fluxes when the heat flux is increased, as observed in other bubble studies [9]. This is due to the increase in nucleation site density, which increases the interaction between nucleation sites. As more nucleation sites become active on the heated surface, bubbles begin to interact.

Figures 8–10 show photographs of the ebullition cycle of three bubbles from inception to collapse. These bubbles nucleate in the highly subcooled region for the following conditions:

Condition reference #	T_{sub} (°C)	$\dot{m}$ (kg s^{-1})	ϕ (MW m^{-2})	Figure
D24	20	0.10	0.3	8
D06	30	0.20	0.5	9
D43	60	0.20	0.9	10

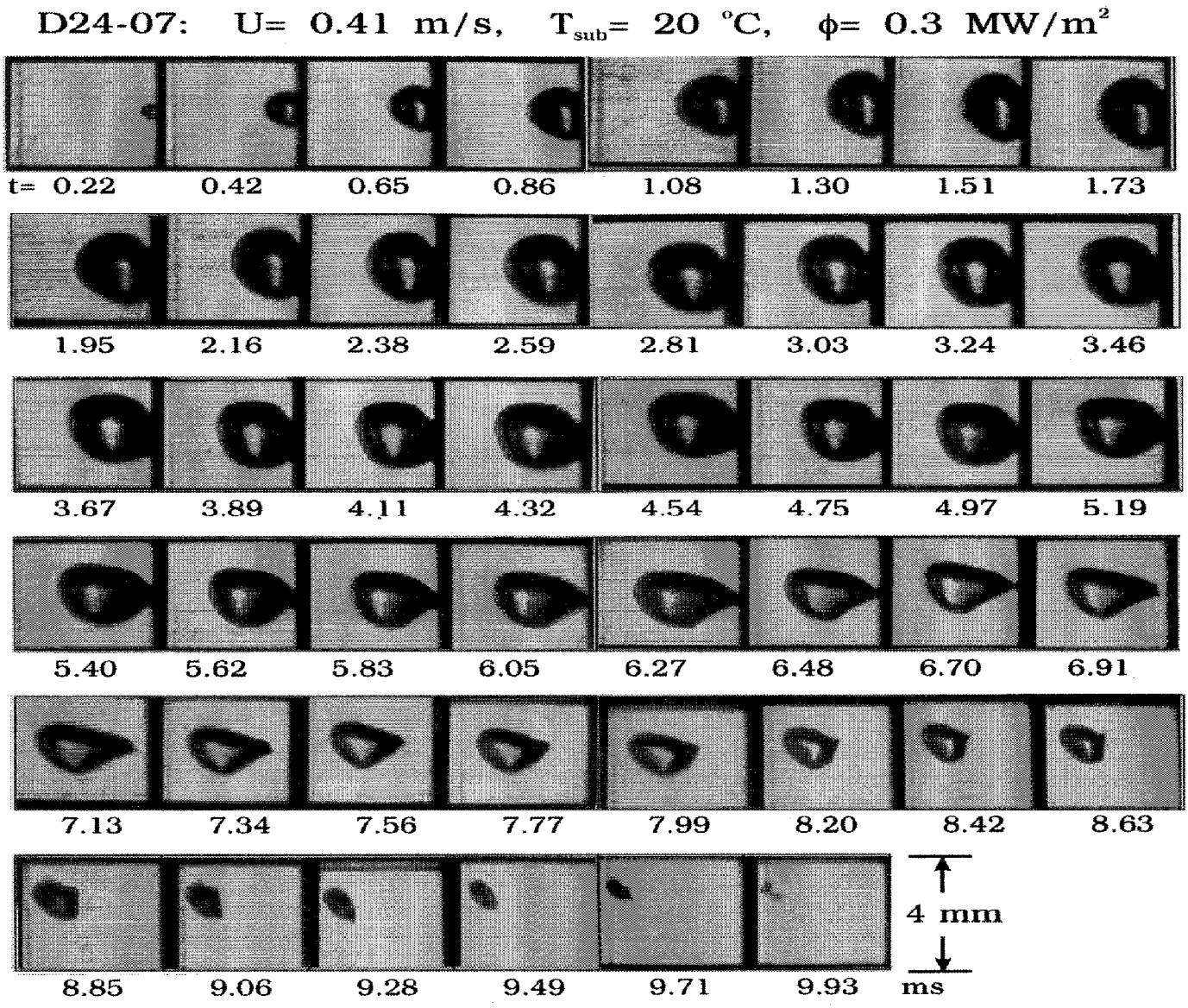

FIG. 8. Photographs of bubble ebullition cycle for reference condition D24.

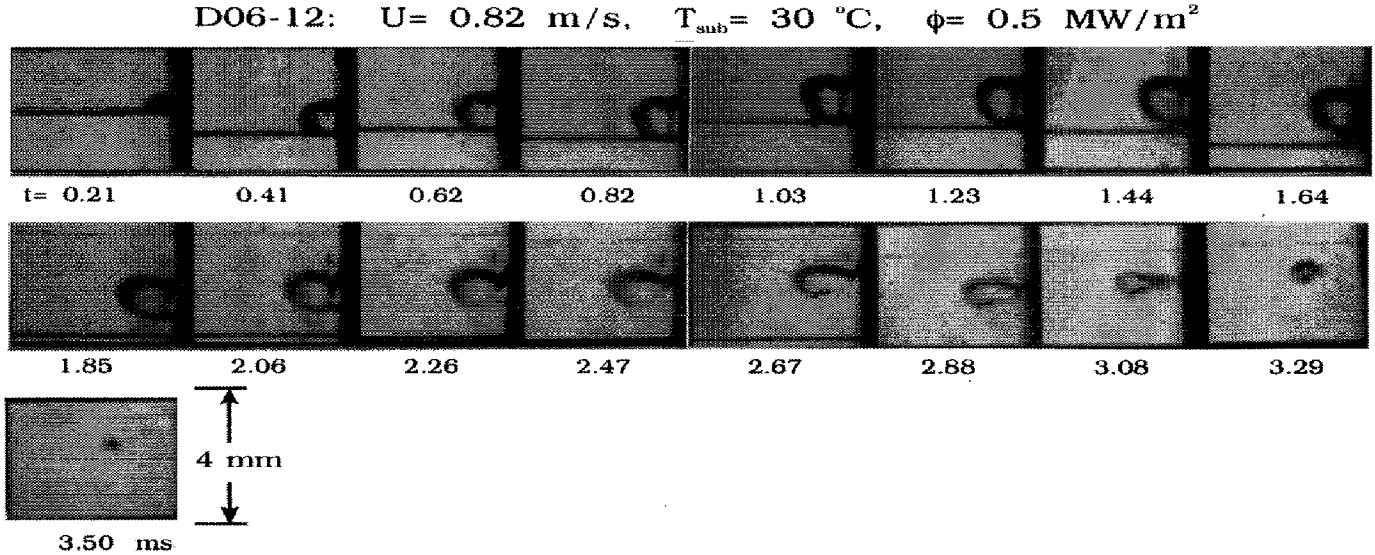

FIG. 9. Photographs of bubble life cycle for reference condition D06.

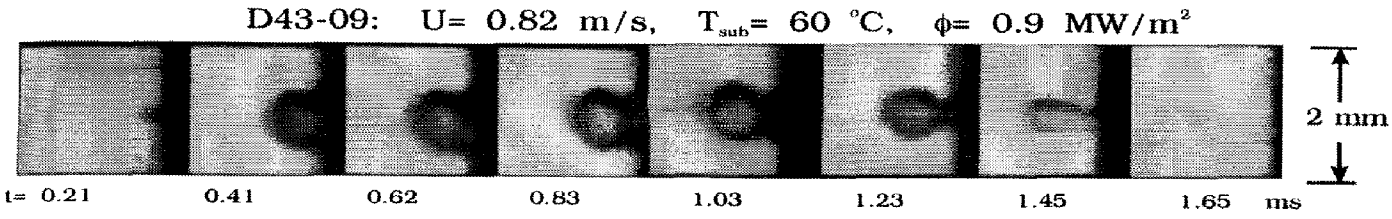

FIG. 10. Photographs of bubble life cycle for reference condition D43.

The condition reference number can be used in conjunction with Fig. 6a–e to locate each of the conditions relative to the ONB and the OSV. The photographed bubbles are shown in the center of each frame in Figs. 8–10 without the reference frame. Therefore, the sliding of the bubble cannot be seen in these figures.† Figure 10 shows the typical bubble behavior at 60°C subcooling.

Figure 11a and b shows the high-speed film digitized results for the bubble radius, R_b, the bubble volume, V_b, and the displacement of the center of mass of the bubble parallel to the heater, L_p, and normal to the heater, L_n^* (defined as L_n minus L_n at ejection). These digitized results are shown as a function of time for reference condition D35 in Fig. 11a, and reference condition D06 in Fig. 11b. The simultaneous presentation of the bubble radius and volume with the displacement of the center of mass of the bubble (normal and parallel to the heater) has not been previously reported in the nucleate boiling literature.

Figures 8–11 show that the initial bubble growth occurs rapidly. This growth is followed by a period where the bubble radius decreases slowly due to condensation. The bubble is slightly flattened for approximately the first-half of the ebullition cycle, with the largest dimension parallel to the wall. At approximately midway in the ebullition cycle, the lower half of the bubble wall starts to converge towards the central normal axis of the bubble until the bubble adheres to the wall at a single point. During this process, the flattened bubble shape becomes elongated, with the largest dimension normal to the wall. Condensation of the bubble also occurs during this transition. The bubble is ejected from the surface after the transition is complete. At ejection, the bubble is shaped like a pear with the stem touching the wall, and is propelled into the core of the flow. After ejection, the bubble condenses rapidly. The lower half of the bubble surface oscillates due to the flow disturbances, while the top portion of the bubble remains approximately hemispherical as the bubble moves towards the fluid core. The oscillation becomes more visible when the film is projected onto a screen and viewed at about 2–6 frames s^{-1}.

Bubbles nucleating close together—before and after the onset of significant void—increase the likelihood of bubble coalescence. Bubbles which coalesce while still sliding along the wall are ejected from the surface together. Individual bubbles are harder to isolate after the onset of significant void. A few bubbles were observed to be ejected into the flow, then bounced back close to the wall and grew again, but this type of bubble behavior was a rare occurrence.

For mean flow velocity of 1.72 m s^{-1}, and pressures of 2 and 3 bar, bubbles slide along the wall soon after nucleation, and are ejected into the flow. The bubble behavior for these conditions is similar to the behavior of bubbles at low velocity and atmospheric pressure, except that the bubbles are much smaller.

In some instances, a bubble will not condense completely, and a very small residual bubble can be observed which eventually condenses or disappears from view. Some of these residual bubbles (less than 0.05 mm dia.) come into view from the bottom of the film, and condense or disappear from view at the top of the frame. These bubbles are believed to hold residual gases.

The bubble life cycle is divided into two main phases which the authors term the *bubble sliding phase* and the *bubble ejection phase*. The two phases are shown in Figs. 11 and 12, and are described separately below.

3.1. *Bubble sliding phase of the ebullition cycle*

The first interval, corresponding to the bubble sliding phase, is assumed to begin immediately upon nucleation, and to finish when the bubble is about to be ejected into the flow. The bubble sliding phase consists of a *growth period* and a *necking period*, as shown in Fig. 12. The growth period starts at bubble inception and ends when the bubble reaches its maximum radius. The necking period starts at the maximum radius and finishes when the bubble is ejected into the flow (i.e. at $t = 6.91$ ms in Fig. 8). The necking period refers to the process after the growth period, when the bubble changes from a flattened shape, becoming elongated while condensing.

Condensation of the bubble starts at the beginning of the necking period, while the bubble is sliding along the wall. The necking period should not be confused with the process of neck formation, which occurs very close to the wall. The existence of a small neck between the bubble and the wall has been debated in the literature [18, 19]. Cooper [19] attributed the observation of a small neck at the base of the bubble to thermal

† The sliding of the bubble is observed from the digitized results in Fig. 11a and b.

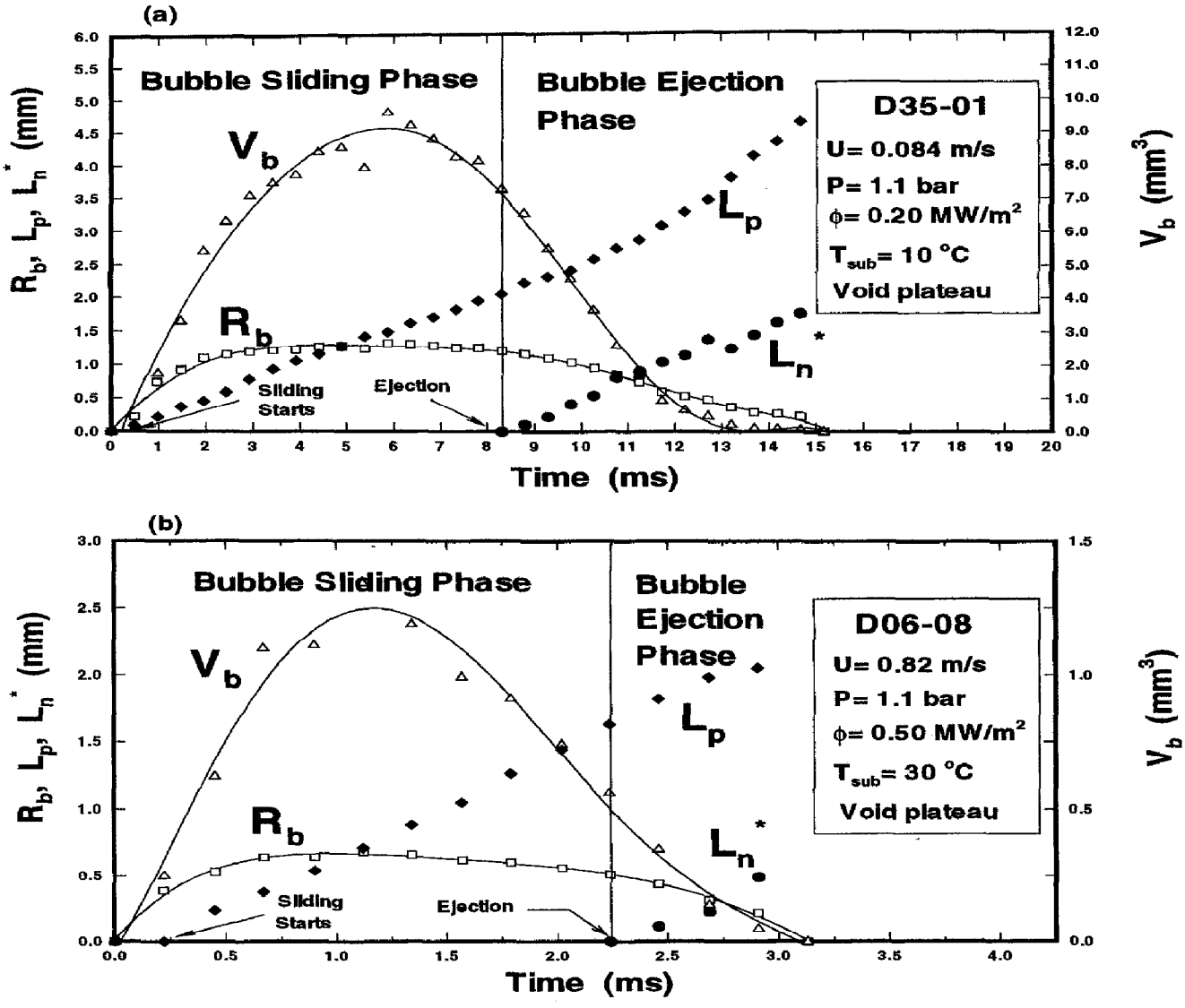

FIG. 11. Bubble radius, volume, and displacement of center of mass of the bubble with respect to the nucleation site and the heated wall, for reference conditions: (a) D35; and (b) D06.

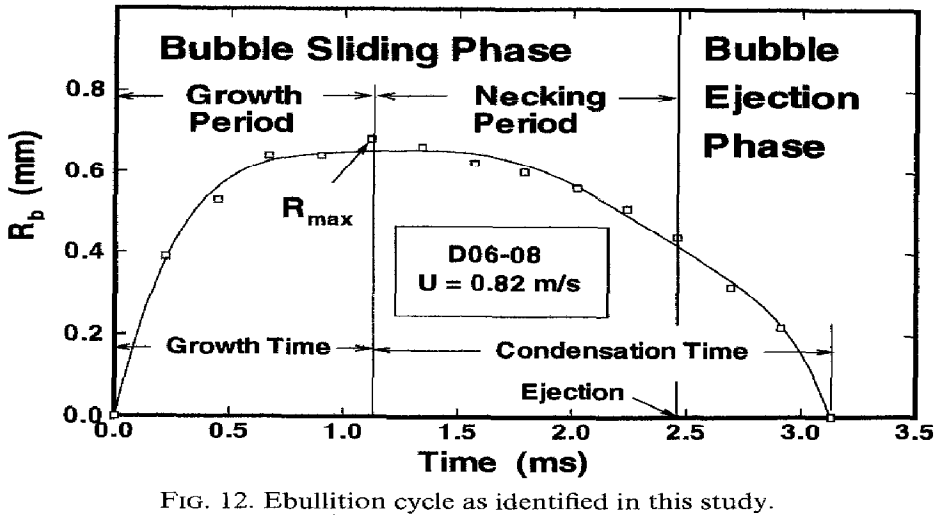

FIG. 12. Ebullition cycle as identified in this study.

gradients at the wall, causing distortion of light and thus producing a 'mirage effect'. This mirage, or reflection at the bubble base, was observed close to the heater in this study when the digitized bubble was magnified by a factor of 36. The bubble base near the wall is not described in this study due to the possible mirage effect.

The bubble slides along the wall during the growth period and the necking period (bubble sliding phase), as evidenced by the positive parallel displacement of the center of mass of the bubble L_p shown in Fig. 11a and b. These figures indicate that bubble sliding occurs almost immediately after nucleation.

Figure 13 shows the diameter of the bubble along the major and minor axis of symmetry, D_p and D_n, with the dynamic contact angles θ_r and θ_a. These results are for the same digitized bubble ebullition cycle as in Fig. 11a. The bubble is flat when D_p is greater than D_n (during the growth period), and is elongated when D_n is greater than D_p (during the necking period). The transition from a flat bubble to an elongated bubble occurs during the necking period. The dynamic receding angle varies between approximately 40 and 70°, while the dynamic advancing angle varies between approximately 45 and 75° during the bubble sliding phase. Accurate measurement of these angles is difficult due to reflection of the bubble interface on the stainless steel heater, and thermal gradients near the heated wall which distort the light.

The axial bubble sliding velocity, u_b, is the slope of the parallel displacement line, L_p. This velocity is relatively constant during the bubble sliding phase (linear variation of the parallel displacement, L_p), and may sometimes vary during the bubble ejection phase (the non-linear change of the parallel displacement, L_p, after ejection), as shown in Fig. 11a. The slip ratio is defined as the average bubble sliding velocity during the bubble sliding phase divided by the mean flow velocity ($S = u_b/U$).

The bubble velocity is influenced by buoyancy for flow velocity less than for the bubble rise velocity. Experimental results from Ivey [20] show that the bubble rise velocity for single vapor bubbles in stagnant water varies from 0.20 to 0.30 m s^{-1} for bubble radii between 0.5 and 2 mm. The influence of buoyancy on the slip ratio is evident in Fig. 11a, where the mean flow velocity ($U = 0.084$ m s^{-1}) is below the bubble rise velocity, and the slip ratio is 3.0. The slip ratio is close to 1 ($S = 0.96$) when the mean flow velocity ($U = 0.82$ m s^{-1}) is greater than the bubble rise velocity, as shown in Fig. 11b. These results are in accordance with previous void fraction measurements for upward and downward flow, which show that the influence of buoyancy is only significant for velocity values less than 0.5 m s^{-1} [21]. Table 3 shows the different values of calculated slip ratio. For flow velocities of 0.42 and 0.82 kg s^{-1}, the slip ratio is close to 1, while, for a flow velocity of 0.082 kg s^{-1}, the slip ratio varies between -0.6 and 3. The variation of the slip ratio, which is highest for $\dot{m} = 0.02$ kg s^{-1}, is attributed to the influence of the bubbles which disturb the flow. The significance of this disturbance increases as the mean flow velocity and the inertial force of the fluid decreases. Flow disturbances caused by the growth and collapse of adjacent vapor bubbles is strong enough for nucleating bubbles to occasionally move in the upstream direction at low flow rate.

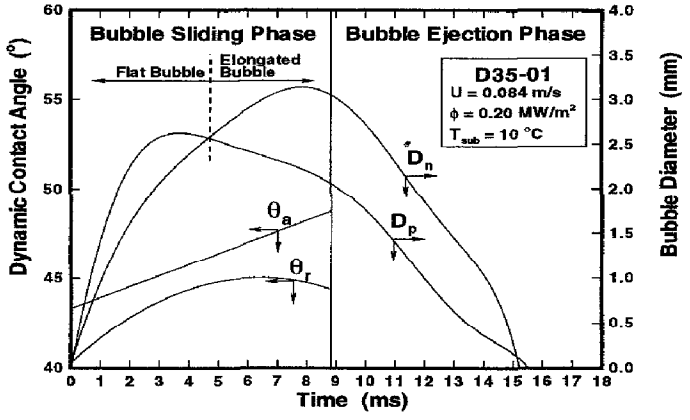

FIG. 13. Bubble dynamic receding and advancing contact angles, and bubble diameter along principal axis parallel to the wall, and normal to the wall, for condition reference D35.

3.2. *Bubble ejection phase of the ebullition cycle*

The bubble ejection phase corresponds to the portion of the ebullition cycle where the bubble is detached from the wall and condenses rapidly in the fluid core. This phase begins when the bubble is ejected from the wall, and ends when the bubble is completely condensed, as shown in Figs. 11a and b and 12. The displacement of the center of mass normal to the wall, L_n^*, is shown in Fig. 11. This displacement is arbitrarily set to zero at ejection, i.e. L_n^* during the ejection phase is defined as the normal distance from the center of mass of the bubble at time 't' to the center of mass of the bubble at ejection.

In the bubble ejection phase, the condensation rate is greater than during the necking period. This can be attributed to three factors: (i) the bubble is no longer absorbing heat from the superheated thermal layer; (ii) the subcooling surrounding the bubble is increasing as the bubble moves away from the wall; and (iii) there is an increase in convection heat transfer at the bubble wall, caused by the normal displacement of the bubble. The convection heat transfer is proportional to the ejection velocity of the bubble u_{ej}, defined as the normal velocity of the center of mass of the bubble. This velocity is reported in Table 3, and the average value for all conditions is 0.75 m s^{-1}. The condensation time was found to be almost independent of the mean flow velocity, since the bubbles travel with the flow [15].

3.3. *Bubble detachment*

Photographic results show that the bubble starts to slide along the wall and eventually is ejected into the flow. Therefore, there are two different bubble detach-

Table 3. High speed photographic results

Condition reference #	T_{sub} (°C)	ϕ (MW m^{-2})	U (m s^{-1})	S	u_{ej} (m s^{-1})	l_{Ptotal} (mm)	l_{Pej} (mm)	t_g/t_b (%)	t_c/t_b (%)	$(t_g+t_n)/t_b$ (%)
D34	10.0	0.1	0.08	1.76	0.15	2.9	2.0	32.8	67.2	36.2
D35	10.0	0.2	0.08	2.99	0.22	4.6	2.6	38.7	61.3	54.8
D36	10.0	0.3	0.08	0.50	0.33	0.5	0.3	32.0	68.0	62.0
D27	20.0	0.2	0.08	4.15	0.60	1.8	−0.3	24.5	75.5	62.3
D28	20.0	0.3	0.08	−0.59	0.64	−1.3	−0.7	38.3	61.7	70.2
D37	30.0	0.2	0.08	1.24	1.13	0.2	0.0	41.2	58.8	76.5
D33	10.0	0.3	0.42	1.40	0.43	5.5	1.5	35.9	64.1	71.8
D24	20.0	0.3	0.42	1.16	0.79	3.7	1.3	36.6	63.4	65.9
D25	20.0	0.6	0.42	1.24	0.95	2.4	0.5	34.5	65.5	69.0
D26	20.0	0.7	0.42	2.00	0.42	4.2	2.4	30.0	70.0	50.0
D05	30.0	0.3	0.42	0.88	0.75	1.6	0.3	29.6	70.4	70.4
D16	30.0	0.6	0.42	1.18	0.93	1.4	0.1	44.5	55.5	88.9
D17	30.0	0.8	0.42	1.36	0.44	1.2	0.0	42.9	57.1	85.7
D18	30.0	0.9	0.42	1.03	1.06	0.6	0.1	30.0	70.0	80.0
D21	20.0	0.6	0.84	1.20	0.59	4.5	2.2	27.3	72.7	50.0
D22	20.0	0.7	0.84	1.05	0.82	3.2	1.1	33.3	66.7	61.9
D06	30.0	0.5	0.83	0.95	1.01	2.0	0.4	35.7	64.3	71.4
D13	30.0	0.8	0.83	0.94	0.98	2.0	0.7	41.2	58.8	64.7
D14	30.0	0.9	0.83	1.16	0.69	2.0	0.5	40.0	60.0	73.4
D39	40.0	0.6	0.83	1.02	1.91	1.6	0.2	33.3	66.7	83.3
D40	40.0	0.9	0.83	0.79	†	1.2	†	42.8	57.2	85.7
D41	40.0	1.2	0.83	1.02	†	1.3	†	44.4	55.6	88.9
D42	60.0	0.6	0.82	0.95	†	0.9	†	37.5	62.5	87.5
D44	60.0	1.2	0.82	0.59	†	0.7	†	28.6	71.4	85.7
Average values				1.2	0.75	2.0	0.6	35	65	71

†Values cannot be determined accurately (only one frame in the ejection region).

ments during the bubble ebullition cycle: detachment from the nucleation site when the bubble starts to slide, and the later detachment from the wall when the bubble is ejected into the flow.

The bubble detachment behavior observed in this photographic study for forced-convective subcooled boiling differs from that reported in the literature. In subcooled boiling [5, 13, 14], detachment has been assumed to occur when the bubble starts to slide away from the nucleation site. A recent study by Klausner *et al.* [22] concluded that, for saturated boiling conditions, bubbles either slide away from the nucleation site, or eject from the nucleation site into the flow (without prior sliding).

The present measurements of the parallel and normal displacement of the center of mass of the bubble show that bubbles always slide along the heater before ejecting. Photographic studies in the literature [5, 22] do not report measurement of the displacement of the center of mass of the bubble. Since the sliding of the bubble may be typically less than 2 mm (before ejection) for a flow velocity of 1.0 m s^{-1}, only an accurate measurement of the displacement of the bubble can provide conclusive evidence on how the bubble detaches. Figure 11a and b, which represents the data processed from photographic films, shows the detachment mechanism in subcooled boiling: bubbles first slide away from the nucleation site, and are then subsequently ejected into the flow.

3.4. *Bubble behavior near the onset of nucleate boiling*

Near the ONB, bubbles behave in a slightly different manner. In films taken at a magnification of 1.0 in which 8 mm of the photographed flow channel appears on each frame of the film, bubbles were seen to slide without being ejected from the wall. It was initially believed that the bubbles grew and collapsed on the wall. No bubbles were observed to nucleate on the wall within the 8 mm photographed length of the heater, and it was not possible to know how far downstream of the photographed area the bubbles nucleated. Bubbles first appeared at the bottom of a frame, and disappeared from view after sliding for 40–50 frames. The bubble radii oscillated while the bubbles slid along the wall. These bubbles were not ejected into the flow, but were sometimes semi-spherical or pear shaped (with the stem on the wall). None of these bubbles was observed to condense completely. To determine the behavior of these bubbles, a film was taken at a magnification of 0.1 so that 80 mm of the heated element was photographed. Projection of the film (at 1–24 frames s^{-1}) showed that these bubbles slide along the test section, sometimes up to a distance of 50 mm, while oscillating in size. After a few oscillations in bubble size and shape, the bubbles are eventually ejected into the flow and then condense very rapidly. Their behavior is analogous to the previous bubble behavior, except that the bubbles near the ONB slide much further along

the wall before being ejected into the fluid core. The period of oscillation varies for each bubble, and does not correspond to the period of a.c. heating. The oscillation in bubble size is probably produced by two conflicting effects: heat gain from the thermal layer and heat loss through condensation.

Figure 14a–c shows the approximate region where bubbles neither grow nor are ejected within the 8 mm (magnification 1:0) photographed section of the heater, for subcoolings of 10, 20 and 30°C. This region is between the ONB line and the *first dashed line*, and is labelled 'bubbles slide more than 8 mm' in the figure. The *second dashed line* in the figure marks the region where the required inlet temperature is less than 15°C. The figure shows that, as the subcooling is increased, the proportion of the highly subcooled region where bubbles slide more than 8 mm decreases. The bubbles generated to the right of the first dashed line in the figure slide 1.4 mm on average. The reason why bubbles slide for a longer distance in the region between the ONB and the first dashed line is due to the lower wall superheat near ONB.

The first region, where bubbles slide for more than 8 mm, is assumed to correspond to the region of partial nucleate boiling; the second region, where bubbles slide 1.4 mm on average, is assumed to correspond to fully-developed boiling, based on observed bubble behavior and subcooled boiling heat transfer characteristics. The heat transfer in the partial nucleate boiling region is influenced by velocity, while the heat

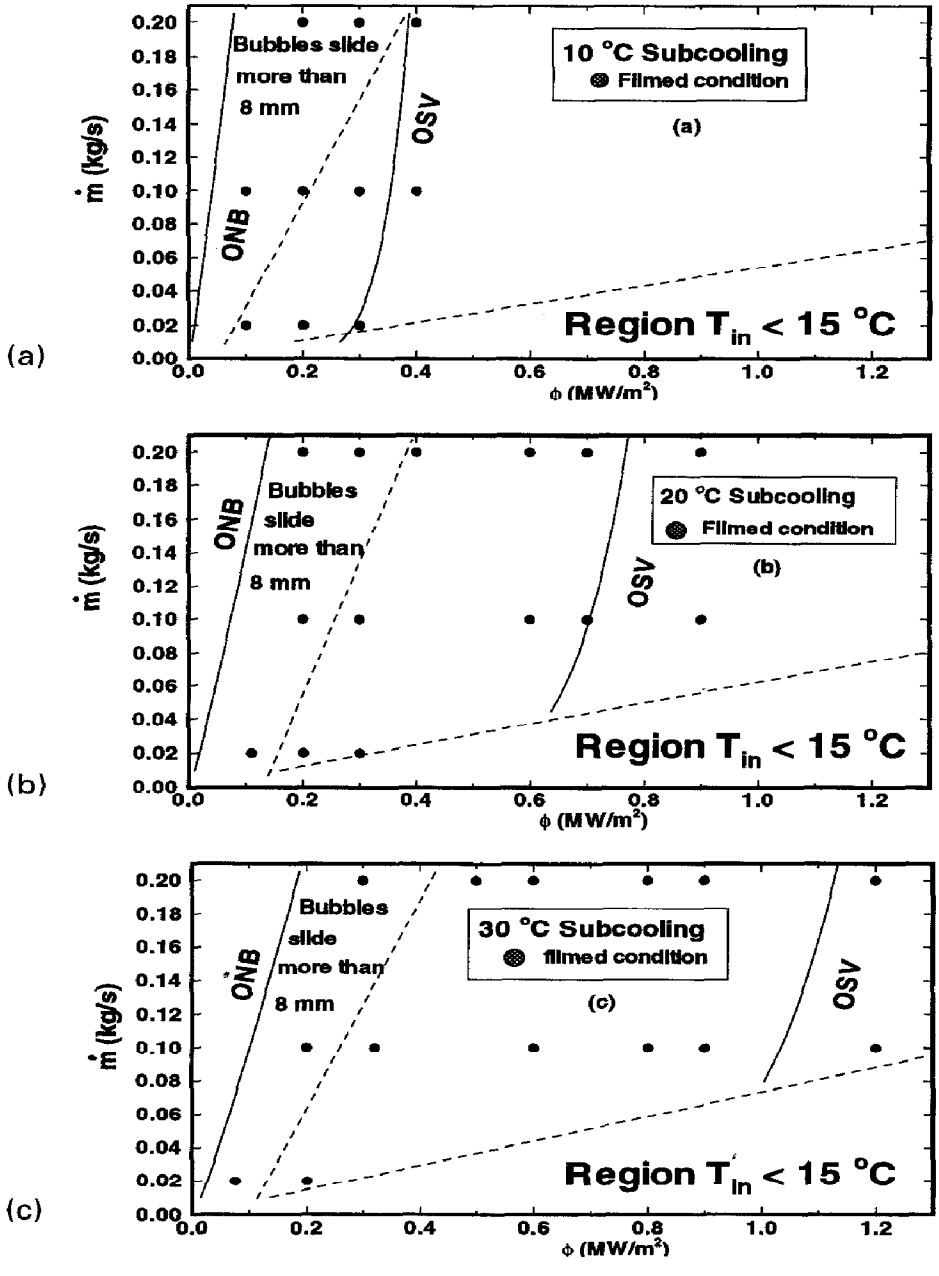

FIG. 14. Different bubble behavior regions in subcooled nucleate boiling for subcoolings of: (a) 10; (b) 20; and (c) 30°C.

transfer mechanism in fully-developed boiling is relatively independent of velocity. The heat transfer mechanism in partial nucleate boiling is assumed to be dominated by bubble sliding and the subsequent mixing of the thermal layer. If bubble sliding is the dominant heat transfer mechanism, then this mechanism is influenced by the flow velocity. As the mean flow velocity increases, the mixing of the thermal layer is promoted by an increase in the bubble sliding velocity, since the slip ratio is close to 1. The heat transfer mechanism in fully-developed nucleate boiling is assumed to be dominated by the ejection of the bubbles agitating the subcooled liquid and the thermal layer. This heat transfer mechanism is fairly independent of velocity since bubbles do not slide for a long distance, even when the velocity is increased. This study introduces the idea that, for subcooled nucleate boiling, bubble sliding may be the dominant heat transfer mechanism in the partial boiling region, and bubble agitation may be the dominant mechanism in fully-developed boiling, although this postulate cannot be confirmed at this time. Latent heat transfer may also be important in the fully-developed boiling region. A comprehensive heat transfer analysis is beyond the scope of this investigation. Based on the experimental results of Gunther [5], Tsung-Chang and Bankoff [3] assume that the heat transfer mechanism in forced-convective subcooled nucleate boiling (partial and fully-developed boiling) is governed by bubble sliding, resulting in an increase in the microlayer evaporation under the bubble. Based on the experimental results of McAdams *et al.* [6], Rohsenow and Clark [4] assume that the mechanism is caused by the agitation of the bubbles.

3.5. *Bubble behavior at high subcooling*

For subcooling values between 10 and 60°C, bubbles do not grow and collapse on the heater. At a subcooling of 60°C, the largest bubbles are clearly ejected into the core of the flow and are pear-shaped prior to ejection. This bubble life cycle is captured on less than 12 frames (less than 3 ms). For smaller bubbles, it is not always possible to capture a bubble in the ejection phase on film, since the ejection process occurs too quickly for this high subcooling. These bubbles show the characteristic elongation normal to the wall (pear-shaped with the stem on the wall), which confirms that these bubbles are ejected into the flow. The present results for subcoolings of 40 and 60°C contradict the results of Gunther [5], who reported that bubbles grow and collapse on the wall for subcoolings greater than 38°C. The different bubble behavior may be due to different test sections. In this investigation, boiling occurs on a stainless steel tube 2.1 mm thick, while, in Gunther's experiment, boiling occurred on both sides of a thin metal strip 0.1 mm thick. Boiling heat transfer from both sides of a thin metal strip may exhibit a different bubble behavior. The bubble life time in Gunther's investigation is less than 0.8 ms,† while the bubble lifetime in this investigation—for subcoolings of 40 and 60°C—is up to five times longer, sufficiently far from the ONB. In addition, Margrini and Nannei [23] found that bubble growth is modified on very thin walls in pool boiling, which suggests that the thin film used by Gunther may produce different bubble behavior than if a thick wall is used. A thick wall tube was chosen in this investigation since it is closer to industrial applications than a thin wall film.

3.6. *Ebullition cycle*

Table 3 shows the axial distance traversed by the bubble from inception to collapse, l_{Ptotal} and from ejection to collapse, l_{Pej}. The average l_{Ptotal} is 2.0 mm and the average l_{Pej} is 0.6 mm. These axial displacement measurements are important for modeling void growth under subcooled boiling conditions since they show that bubbles do not travel far downstream; the influence of the bubble is confined locally to a small portion of heater element.

Figure 15 shows two successive bubble ebullition cycles, with different times describing each phase of the ebullition cycle. The cycle represents a typical bubble behavior in subcooled boiling. The figure shows the bubble growth time, t_g, necking time, t_n, condensation time, t_c, and lifetime, t_b. The bubble period, t_p, is the time between two successive nucleations, and the bubble waiting time, t_w, is defined as the time between bubble ejection and the nucleation of a new bubble, where $t_w = t_p - t_n - t_g$. As stated previously, the bubble starts to condense after R_{max}.

In general, the bubble ejection phase has a shorter duration than the bubble sliding phase (Fig. 11b) except at low subcooling (Fig. 11a). Table 3 shows that, on average, 35% of the bubble ebullition cycle is occupied by the growth period (t_g/t_b), condensation occurs during 65% (t_c/t_b) of the ebullition cycle, and the bubble slides along the wall for 71% of the ebullition cycle ($(t_g + t_n)/t_b$).

3.7. *Maximum radius and bubble lifetime*

Figure 16 shows the variations of the maximum radius, R_{max}, and the bubble lifetime, t_b, as functions of heat flux for a constant subcooling and at mean flow velocities of 0.41 and 0.82 m s^{-1}. Both the maximum radius and bubble lifetime decrease with heat flux. The maximum radius and the bubble lifetime are relatively independent of flow velocity, as reported in ref. [15].

At constant subcooling, the maximum radius and bubble lifetime decrease as the heat flux is increased due to an increase in the wall superheat, thus causing an increase in the nucleation site density. As more bubbles are produced on the wall, there is more competition for the wall heat flux, and thereby less heat

† Gunther had to use a film speed of 20 000 frames s^{-1} to capture the bubble ebullition cycle on film, while in this investigation a film speed of 6000 frames s^{-1} was adequate for most cases.

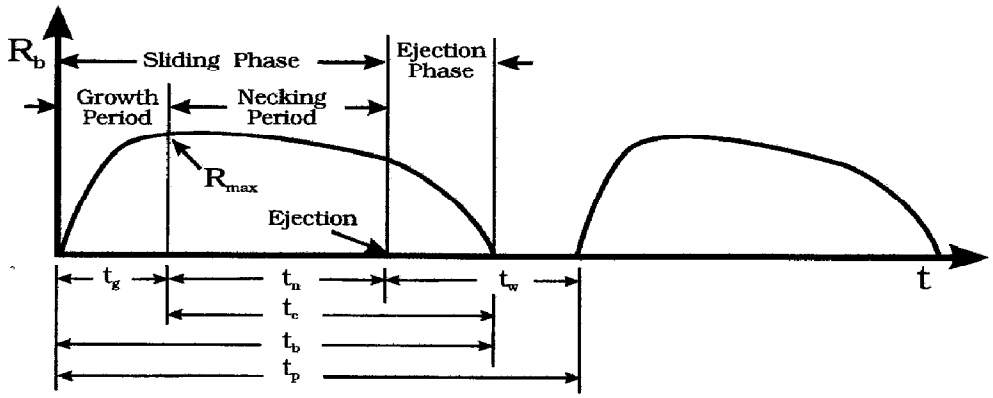

FIG. 15. Time definitions.

flux available to each bubble. Interaction among the bubbles increases as the heat flux is increased, which leads to a homogenization of the bubble parameters. Results show that as the OSV is approached, changes in heat flux do not significantly affect the bubble size and lifetime at a given subcooling. Similarly, the bubble lifetime decreases as the heat flux increases, since the maximum radius decreases. The decrease in bubble radius and lifetime with increasing heat flux has been observed by Gunther [5] for bubbles which grow and condense on the wall at high subcooling.

Figure 17 shows the variation of the maximum radius and the bubble lifetime as a function of subcooling for a constant heat flux of 0.3 MW m^{-2}, and for flow velocities of 0.082 and 0.41 m s^{-1}. The figure shows that an increase in subcooling may either increase or decrease the maximum bubble radius or the bubble lifetime at constant heat flux. In general, an increase in subcooling should result in a decrease in both of these parameters, since the fluid surrounding the bubble is cooler. However, bubble size and lifetime may actually increase when the subcooling is increased for a constant heat flux, due to a reduction in interaction among nucleation sites. The figure shows the condition reference number beside each data point, allowing a cross-reference with Fig. 6a–e in order to locate the relative position with respect to either the ONB or the OSV. The bubble lifetime and size depend on its relative position within the highly subcooled region. The bubble formed for reference condition number D36 (10°C subcooling) is at the onset of significant void, where there is substantial bubble interaction among the nucleation sites. The bubble formed for reference condition number D28 (20°C subcooling) is for a higher subcooling than for reference condition D36; the maximum bubble radius, however, is larger. For condition D28, the bubbles nucleate closer to the onset of nucleate boiling, where there is less interaction between nucleation sites. There appear to be two opposing trends which determine the effect on the bubble size and lifetime when the subcooling is increased at constant heat flux. First, the increase in subcooling reduces the heat content of the fluid surrounding the bubble, which

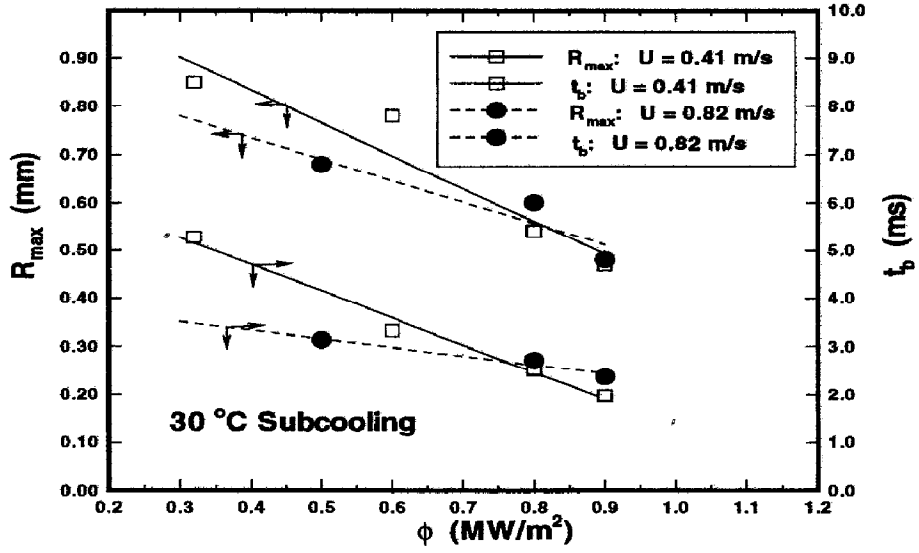

FIG. 16. Effect of heat flux on bubble maximum radius and lifetime.

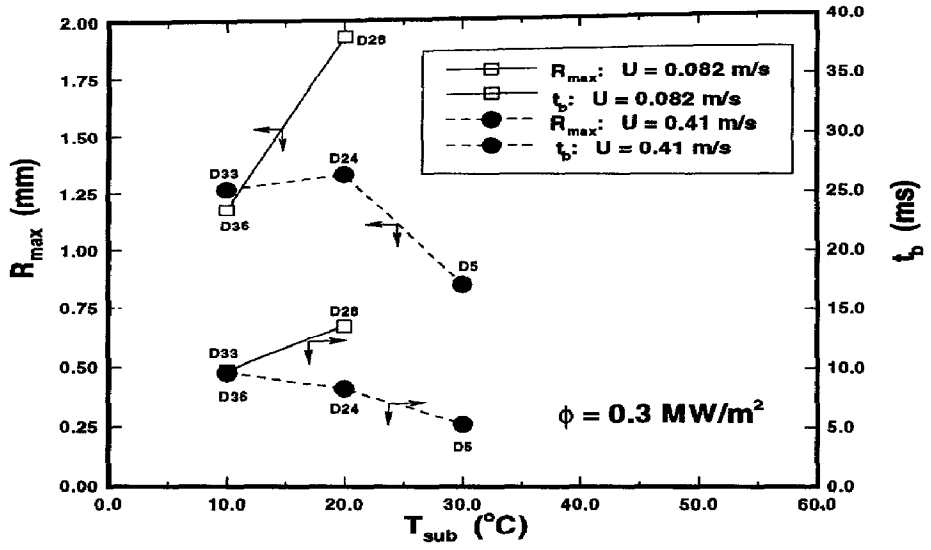

FIG. 17. Effect of subcooling on bubble maximum radius and lifetime.

decreases the size of the bubble and its lifetime. Second, the increase in subcooling moves the bubble condition away from the OSV towards ONB, decreasing the nucleation site density and thus increasing the bubble maximum radius and lifetime. Larger bubbles are formed to dissipate the same amount of heat flux when fewer nucleation sites are active.

This variation in the bubble size and lifetime with respect to subcooling has not been previously documented for low- and medium-subcooled conditions. However, non-monotonic changes in a bubble's characteristics as a function of subcooling were previously reported for pool boiling conditions. The effect of subcooling on the frequency of bubble emission was investigated for pool boiling conditions by Ibrahim and Judd [24], and Judd [25]. Results showed that the bubble emission frequency first increased and then decreased as the subcooling was increased. A heat transfer model was developed to predict this behavior, taking nucleation site density into account.

4. CONCLUSIONS

A high speed photographic study was carried out for different values of heat flux (0.1–1.2 MW m^{-2}), subcooling (10, 20, 30, 40 and 60°C), and flow rate (0.02, 0.10 and 0.20 kg s^{-1}) to investigate the ebullition of vapor bubbles in subcooled nucleate boiling at atmospheric pressure. The following conclusions can be drawn:

1. Bubble growth occurs rapidly, and is followed by a period when the bubble radius remains relatively constant. During bubble growth, the inertial forces cause the bubble to have a slightly flattened shape. Bubbles start to slide away from their nucleation sites almost immediately after nucleation, with a slip ratio close to 1.
2. After the onset of nucleate boiling, bubbles detach from the nucleation site and start to slide, then later detach from the heated wall as they are ejected into the flow.
3. Bubbles become elongated as they slide on the wall, and are shaped like an inverted pear with the stem touching the wall just prior to ejection.
4. The bubble diameter at ejection is smaller than the maximum diameter, since the bubble condenses on the wall while sliding. The maximum diameter varies between 0.8 and 3.0 mm.
5. Bubble behavior is mapped into two regions for increasing heat flux for constant values of subcooling and flow rate. The first region occurs near the onset of nucleate boiling, where bubbles slide along the wall for more than 8 mm and up to a distance of 50 mm, and oscillate in size before being ejected. The second region occurs well after the onset of nucleate boiling, where the average maximum axial distance the bubbles slide along the wall prior to ejection is 1.4 mm. In this region, the average axial distance traversed by the condensing bubbles after ejection is 0.6 mm.
6. Bubbles do not grow and collapse on the heated wall for the range of subcooling investigated (10–60°C).

Acknowledgments—We would like to thank D. Farajisarir for his contribution in developing the high speed photographic and digital analysis experimental setup. Valuable suggestions from Dr Yacov Barnea during the high speed photographic study are greatly appreciated. We acknowledge Deborah Varley for helping in editing the paper. This work was funded by the Natural Sciences and Engineering Research Council of Canada and the Atomic Energy of Canada Limited.

REFERENCES

1. S. Z. Rouhani and E. Axelsson, Calculation of void volume fraction in the subcooled and quality boiling regions, *J. Heat Transfer* **13**, 383–393 (1970).

2. R. W. Bowring, Physical model, based on bubble detachment, and calculation of steam voidage in the subcooled region of a heated channel, HPR-29. Institutt for Atomenergi, Halden, Norway (1962).
3. G. Tsung-Chang and S. G. Bankoff, On the mechanism of subcooled nucleate boiling, *J. Heat Transfer* **112,** 213–218 (1990).
4. W. M. Rohsenow and J. A. Clark, A study of the mechanism of boiling heat transfer, *Trans. ASME* **73,** 609–620 (1951).
5. F. C. Gunther, Photographic study of surface-boiling heat transfer to water with forced convection, *Trans. ASME* **73,** 115–123 (1951).
6. W. H. McAdams, W. E. Kennel, C. S. Minden, C. Rudolf, P. M. Picornell and J. E. Dew, Heat transfer at high rates to water with surface boiling, *Indust. Engng Chem.* **41** (1949).
7. S. V. Sralen, Effect of vapor-bubble behavior on heat transfer in two-phase flow of pure and binary systems. In *Boiling Phenomena* (Edited by S. V. Stralen and R. Cole), Vol. 2, pp. 669–777. McGraw-Hill (1979).
8. M. Akiyama and F. Tachibana, Motion of vapor bubbles in subcooled heated channel, *Bull. JSME* **17,** 241–247 (1974).
9. V. H. Del Valle and D. B. R. Kenning, Subcooled flow boiling at high heat flux, *Int. J. Heat Mass Transfer* **28,** 1907–1920 (1985).
10. G. E. Dix, Vapor void fraction for forced convection with subcooled boiling at low flow rates, Ph.D. Thesis, University of California, Berkeley (1971). Also, General Electric Report Number NEDO-10491.
11. H. C. Unal, Determination of the initial point of net vapor generation in flow boiling systems, *Int. J. Heat Mass Transfer* **18,** 1095–1099 (1975).
12. R. Cole, Nucleate-boiling heat transfer, a general survey. In *Boiling Phenomena* (Edited by S. V. Stralen and R. Cole), Vol. 1, p. 162. McGraw-Hill (1979).
13. S. Levy, Forced convection subcooled boiling—prediction of vapor volumetric fraction, *Int. J. Heat Mass Transfer* **10,** 951–965 (1967).
14. J. T. Rogers, M. Salcudean, Z. Abdullah, D. Mcleod and D. Poirier, The onset of significant void in upflow boiling of water at low pressure and velocities, *Int. J. Heat Mass Transfer* **30,** 2247–2260 (1987).
15. D. Farajisarir, Bubble dynamics in subcooled flow boiling, Master's Thesis, Dept. Mech. Eng., University of British Columbia (1993).
16. E. L. Bibeau, M. Salcudean and J. E. Kowalski, Subcooled void growth for finned and annular geometries at low velocities and low pressures, Third World Conference on Experimental Heat Transfer, Fluid Mechanics and Thermodynamics, Hawaii (1993).
17. E. L. Bibeau, Void growth in subcooled flow boiling for circular and finned geometries for low values of pressure and velocity, Ph.D. Thesis, University of British Columbia (1993).
18. M. G. Cooper and T. T. Chandratilleke, Growth of diffusion-controlled vapor bubbles at a wall in a known temperature gradient, *Int. J. Heat Mass Transfer* **24,** 1475–1492 (1981).
19. M. G. Cooper, The mirage in boiling, *Int. J. Heat Mass Transfer* **26,** 1088–1090 (1983).
20. H. J. Ivey, Relationships between bubble frequency, departure diameter and rise velocity in nucleate boiling, *Int. J. Heat Mass Transfer* **10,** 1023–1040 (1967).
21. E. L. Bibeau and M. Salcudean, The effect of flow direction on void growth at low velocities and low pressure, *Int. Comm. Heat Mass Transfer* **17,** 19–25 (1990).
22. J. F. Klausner, R. Mel, M. Bernhard and L. Z. Zeng, Vapor bubble departure in forced convection boiling, *Int. J. Heat Mass Transfer* **36,** 651–662 (1993).
23. U. Magrini and E. Nannei, On the influence of the thickness and thermal properties of heating walls on the heat transfer coefficients in nucleate boiling, *J. Heat Transfer* **97,** 173–178 (1975).
24. E. A. Ibrahim and R. L. Judd, An experimental investigation of the effect of subcooling on bubble growth and waiting time in nucleate boiling, *J. Heat Transfer* **107,** 168–174 (1985).
25. R. L. Judd, The influence of subcooling on the frequency of bubble emission in nucleate boiling, *J. Heat Transfer* **111,** 747–754 (1989).